Association of locus coeruleus integrity with Braak stage and neuropsychiatric symptom severity in Alzheimer's disease

Running title: Locus coeruleus integrity in Alzheimer's disease

Clifford M Cassidy[1,2,3†], Joseph Therriault[2,3,4,5], Tharick A Pascoal[2,3,4,5,6], Victoria Cheung[1], Melissa Savard[2,3,4,5], Lauri Tuominen[1], Mira Chamoun[2,3,4,5], Adelina McCall[1], Seyda Celebi[1], Firoza Lussier[2,3,4,5], Gassan Massarweh[4,6], Jean-Paul Soucy[4,6], David Weinshenker[7], Christine Tardif[4,6], Zahinoor Ismail[8], Serge Gauthier[2,9], Pedro Rosa-Neto[2,3,4,5,6]

1. The Royal's Institute of Mental Health Research, affiliated with The University of Ottawa, Ottawa, Canada
2. Translational Neuroimaging Laboratory, The McGill University Research Centre for Studies in Aging, McGill University, Montreal, Canada.
3. Douglas Research Institute, Le Centre intégré universitaire de santé et de services sociaux (CIUSSS) de l'Ouest-de-l'Île-de-Montréal, McGill University, Montreal, Canada.
4. Department of Neurology and Neurosurgery, McGill University, Montreal, Canada.
5. Department of Psychiatry, McGill University, Montreal, Canada.
6. Montreal Neurological Institute, McGill University, Montreal, Canada.
7. Department of Human Genetics, Emory University School of Medicine, Atlanta, GA.
8. Hotchkiss Brain Institute, University of Calgary, Calgary, Canada
9. Alzheimer's Disease Research Unit, The McGill University Research Centre for Studies in Aging, McGill University, Montréal, QC, Canada

†Corresponding author:
Clifford Cassidy, 1145 Carling Ave, Ottawa ON, Canada K1Z 7K4.
clifford.cassidy@theroyal.ca

Abstract

The clinical and pathophysiological correlates of locus coeruleus (LC) degeneration in Alzheimer's disease (AD) could be clarified using a method to index LC integrity in vivo, neuromelanin-sensitive MRI (NM-MRI). We examined whether integrity of the LC-norepinephrine system, assessed with NM-MRI, is associated with stage of AD and with neuropsychiatric symptoms (NPS), independent of cortical pathophysiology (amyloid-β and tau burden). Cognitively normal older adults (n=118), and individuals with mild cognitive impairment (MCI, n=44), and AD (n=28) underwent MR imaging and tau and amyloid-β positron emission tomography (with [^{18}F]MK6240 and [^{18}F]AZD4694, respectively). Integrity of the LC-norepinephrine system was assessed based on contrast-to-noise ratio of the LC on NM-MRI images. Braak stage of AD was derived from regional binding of [^{18}F]MK6240. NPS were assessed with the Mild Behavioral Impairment Checklist (MBI-C). LC signal contrast was decreased in tau-positive participants (t_{186}=-4.00, p=0.0001) and negatively correlated to Braak stage (Spearman ρ=-0.31, p=0.00006). In tau-positive participants (n=51), higher LC signal predicted NPS severity (ρ=0.35, p=0.019) independently of tau burden, amyloid-β burden, and cortical gray matter volume. This relationship appeared to be driven by the impulse dyscontrol domain of NPS, which was highly correlated to LC signal (ρ=0.44, p=0.0027). NM-MRI reveals loss of LC integrity that correlates to severity of AD. However, LC preservation in AD may also have negative consequences by conferring risk for impulse control symptoms. NM-MRI shows promise as a practical biomarker that could have utility in predicting the risk of NPS or guiding their treatment in AD.

Introduction

The locus coeruleus (LC), the primary site of norepinephrine neurons in the human brain, is an important site of neurodegeneration in Alzheimer's disease (AD) [1,2]. Neuropathological studies have found that the LC is the first brain region to accumulate hyperphosphorylated tau proteins years prior to the onset of cognitive impairment and clinical diagnosis [2-4], and post-mortem data suggest that degeneration of the LC in AD may be a slow and gradual process that is delayed relative to the early accumulation of LC tau [1]. Although the LC is clearly implicated in AD, challenges studying LC physiology in humans *in vivo* have limited our understanding of the timing of LC changes and their association with characteristic aspects of AD pathophysiology and clinical features.

Neuromelanin-sensitive MRI (NM-MRI) [5] provides a practical means to overcome this obstacle by using neuroimaging to investigate the integrity of the LC in living human brain. This brief and non-invasive scan yields a high signal contrast in the LC, presumably due to its high concentration of neuromelanin (NM), a paramagnetic pigment [5,6], although the relative contributions of various components of the signal are still under debate and investigation [7-9]. Reduced LC NM-MRI signal is associated with smaller LC volume postmortem [6], loss of norepinephrine terminals in the brain [10], AD diagnosis [7,11-14], and CSF amyloid-β levels [15], strongly suggesting low LC NM-MRI signal is indicative of degeneration of norepinephrine LC neurons. While previous studies have demonstrated the utility of NM-MRI in AD [7,11-14]. and shown correlation to tau burden [8], further multimodal imaging work is needed to determine the contribution of LC degeneration to key features of the illness independent of amyloid-β and tau burden and gray matter atrophy. To support this, the validated [16,17] radiotracers [^{18}F]AZD4694 [18] (for amyloid-β) and [^{18}F]MK6240 [19] (for tau) allow *in vivo* AD diagnosis and Braak Staging [20-22].

Consistent with the known functions of the norepinephrine system, changes in the LC-norepinephrine system have been implicated in cognitive deficits and neuropsychiatric symptoms (NPS) in patients with AD [2,3] and animal models [2,23]. NPS are a common and burdensome aspect of Alzheimer's disease (AD) [24,25] that often emerge early in the course of the illness [26-28], render patients more likely to require residential care [29,30], and are not easily treatable [29,31-33]. Norepinephrine disturbances correlate to NPS in AD [24,34-37] and may have a causal role because symptoms of agitation/aggression [38-40] and depression [41] respond to treatment with drugs targeting the norepinephrine system. The nature of LC dysfunction in AD may be complex, and compensatory changes may occur in response to LC degeneration, possibly even leading to hyperactivity in remaining LC neurons [2,3,36,42,43]. Indeed, cerebrospinal fluid levels of norepinephrine and biosynthetic capacity of norepinephrine (indexed as tyrosine hydroxylase expression) are elevated in AD despite LC degeneration [42-44]. These changes may have negative consequences in AD as some types of NPS, including agitated, aggressive, and psychotic symptoms and prescription of neuroleptic agents, have been linked to *high or preserved* norepinephrine function [34,36-40,45] and can respond to norepinephrine-system blocking medication [38,39]. Although no prior NM-MRI studies have investigated NPS in AD, in other populations the NM-MRI signal correlates to behaviors resembling aspects of NPS including depression [46], sleep disturbance [47], and autonomic nervous system function [48].

Similarly to norepinephrine function, cortical pathology, including aggregation of amyloid-β [19,49] and phosphorylated tau [27,50,51], is also linked to NPS severity in AD. Thus, disentangling the pathophysiological correlates of NPS may require simultaneous examination of these different insults to determine their independent contributions to the emergence of NPS. We postulate that NPS reflect an imbalance in specific aspects of AD pathophysiology: integrity of the LC on one hand and amyloid-β and tau accumulation in the cortex on the other hand. The combined effects of these processes may lead to a disruption in cortical and subcortical regulation of behavior, promoting emergence of NPS. Identifying neuroimaging measures that strongly predict NPS would not only help understand the mechanism of their pathogenesis but would also support the effort to find biomarkers to assess NPS risk, guide prescription of existing treatments or advance trials of novel treatments.

Here we combine these advanced neuroimaging methods with assessment of NPS using the validated Mild Behavioral Impairment Checklist (MBI-C) [52] an instrument that is sensitive and specific in capturing a broad spectrum of NPS in older adults across the cognitive spectrum from cognitively normal older adults through to moderate AD [53,54]. We hypothesize that LC signal will be reduced in AD but correlate positively to NPS severity.

Materials and methods

Participants and clinical measures

Study participants from the community or outpatients at the McGill University Research Centre for Studies in Aging were enrolled in the Translational Biomarkers of Aging and Dementia (TRIAD) cohort [55], McGill University, Canada. The cohort participants had a detailed clinical assessment, including the Clinical Dementia Rating Scale (CDR) and Mini-Mental State Examination (MMSE). Cognitively unimpaired participants had no objective cognitive impairment and a CDR score of 0. Mild cognitive impairment (MCI) individuals had subjective and objective cognitive impairment, preserved activities of daily living, and a CDR score of 0.5. Patients with mild-to-moderate sporadic Alzheimer's disease dementia had a CDR score between 0.5 and 2, and met the National Institute on Aging and the Alzheimer's Association criteria for probable Alzheimer's disease determined by a physician.[56] Participants were excluded if they had other inadequately treated conditions, active substance abuse, recent head trauma, or major surgery, or if they had MRI/PET safety contraindication. Alzheimer's disease patients did not discontinue medications for this study.

NPS severity was assessed using the MBI-C, http://www.MBItest.org [52]. The participant's primary informant, most frequently their spouse, completed the MBI-C. The MBI-C is composed of 34 questions and subdivided into five domains: decreased drive and motivation, affective dysregulation, impulse dyscontrol (agitation, impulsivity, and abnormal reward salience), social inappropriateness, and abnormal perception/thought content. Each question answered "Yes" is accorded a severity rating (1=mild, 2=moderate, or 3=severe). To be endorsed, symptoms must have emerged later in life and persisted for minimum 6 months continuously or intermittently. The Douglas Institute Research Ethics Board approved this study; all participants provided written informed consent.

MRI Acquisition

All neuroimaging data were acquired at the Montreal Neurological Institute (MNI). Magnetic resonance (MR) images were acquired on a 3T Prisma scanner. NM-MRI images were collected

via a turbo spin echo (TSE) sequence with the following parameters: repetition time (TR)=600 ms; echo time (TE)=10 ms; flip angle=120°; turbo factor=4; in-plane resolution=0.6875×0.6875 mm^2; partial brain coverage overlaying the pons and midbrain with field of view (FoV)=165×220; number of slices=20; slice thickness=1.8 mm; number of averages=7; acquisition time=8.45 min. Whole-brain, T1-weighted MR images (resolution=1 mm, isotropic) were acquired using an MPRAGE sequence for preprocessing of the NM-MRI and PET data. Quality of MRI images was visually inspected for artifacts immediately upon acquisition, and scans were repeated when necessary, time permitting. Cortical gray matter volume and estimated total intracranial volume were obtained using FreeSurfer version 6.0 (Martinos Center for Biomedical Imaging) standard segmentation pipeline.

Preprocessing of NM-MRI images

LC signal was measured for the whole LC and LC subregions (rostrocaudal sections) using a semi-automated algorithm incorporating steps similar to those described in previous studies [47,57]. This method performs an intensity-threshold-free cluster search within an overinclusive mask of the LC in native space. For simplicity we refer to it as a 'funnel tip' method, see Figure 1 for summary of the steps in the algorithm. Although LC signal is measured on native-space NM-MRI images, it is necessary to spatially normalize the NM-MRI images in order to register an overinclusive LC mask (referred to as the LC search mask) from MNI space to native space for each participant. Initial preprocessing steps were performed as in our prior work examining NM-MRI signal from the substantia nigra [58,59] using ANTs software. To bring the NM-MRI image of each participant into standardized space, T1-weighted images were normalized to MNI space, then NM-MRI images were coregistered to the T1-weighted images, and finally these two transforms were applied to the NM-MRI images. A visualization template (Figure 1) was created by averaging the spatially normalized NM-MRI images from all participants.

Subsequent steps used custom Matlab scripts. An LC search mask was drawn over the MNI-space visualization template to cover the LC, defined as the hyperintense voxels at the anterior-lateral edge of the 4th ventricle spanning 15 mm in the rostrocaudal axis (from MNI space coordinates z= -16 to -31, see Figure 1). The rostrocaudal limits were set based on the position of the LC from a brainstem atlas[60] and cell counting work [61], spanning from the inferior collicus to the posterior recess of 4th ventricle, while excluding the extreme rostral and caudal ends to minimize edge effects. The mask was divided into 5 rostrocaudal sections of equal length (3 mm). The full LC search mask and the 5 mask sections were then warped to native space using the inverse transformation generated in the spatial normalization step and resampled to NM-MRI image space. This warped LC search mask defined a search space wherein to find the LC for each participant. A cluster-forming algorithm was used to segment the LC within this space, defined as the 4 contiguous voxels (total area=1.96 mm^2) on each side and axial slice with the highest mean signal. To minimize partial volume effects, only the peak intensity voxel of these 4 was retained for calculation of LC signal (on the assumption that this voxel had the highest fraction of LC tissue). The automated segmentation was visually inspected and was found to perform 2.2% of operations suboptimally (e.g. by locating the LC within a bright artifact occasionally present within the 4th ventricle), requiring manual correction. Contrast-to-noise ratio (CNR) for each voxel *v* in a given axial slice was then calculated as the relative difference in NM-MRI signal intensity *I* from a reference region *RR* in the same slice as: $CNR_{\mathrm{v}} = (I_v - mode(I_{RR}))/mode(I_{RR})$. We used a reference region with low NM

concentration, the central pons (Figure 1, similar to previous work)[62], defined by a circle of radius 11.6 mm, centered on the midline, 32.6 mm anterior to the LC. Finally, every LC-containing slice was linked to one of the 5 rostrocaudal LC sections based on which of the 5 sectioned LC masks was present on the same axial slice (if 2 sectioned masks were present on the same slice, the LC section was defined for each side by the sectioned mask covering the most LC voxels). LC signal was calculated for each of the five sections by averaging CNR values from all LC voxels within the section.

PET Acquisition and Analysis

All individuals had [^{18}F]AZD4694 and [^{18}F]MK6240 PET scans acquired with a brain-dedicated Siemens High Resolution Research Tomograph (HRRT). See previous studies for more detailed PET methods [18,19]. Tau [^{18}F]MK6240 images were acquired at 90–110 min after the intravenous bolus injection of the tracer and were reconstructed using an OSEM algorithm on a 4D volume with four frames (300 s each) [63]. Amyloid-β [^{18}F]AZD4694 images were acquired at 40–70 min after the intravenous bolus injection of the tracer, and scans were reconstructed with the same OSEM algorithm on a 4D volume with three frames (600 s each) [64]. At the end of each PET acquisition, a 6-min transmission scan was conducted with a rotating ^{137}Cs point source for attenuation correction. The images were corrected for dead time, decay, random and scattered coincidences, and for motion. In order to normalize the PET data, T1-weighted MRIs were non-uniformity and field distortions corrected. PET images were then automatically registered to T1-weighted image space, and the T1-weighted images were linearly and non-linearly registered to the ADNI standardized space [65]. PET images were meninges- and skull-stripped and non-linearly registered to the ADNI template using the transformations from the T1-weighted image to ADNI template and from the PET image to T1-weighted image space. [^{18}F]MK6240 standardized uptake value ratio (SUVR) and [^{18}F]AZD4694 SUVR maps were calculated using the inferior cerebellum and whole cerebellum grey matter as the reference region, respectively [63,64]. PET images were spatially smoothed to achieve a final 8-mm full-width at half-maximum resolution. [^{18}F]MK6240 values were extracted from a temporal ROI used previously to define tau positivity [66] (we refer to this as the 'temporal ROI'; see Figure 2D). Tau positive cases were defined as those with SUVR >1.24 in the temporal ROI, as in our prior work using this threshold to define tau positivity [21]. A continuous measure of SUVR from this ROI was also included in several analyses. Subjects were divided into Braak stage groups [67-70] according to [^{18}F]MK6240 SUVR values in Braak stage ROIs using methods previously employed by our group [22]. Discordant cases (where regional tau burden did not follow the anatomical progression proposed by Braak) were excluded from analyses of Braak stage. Global [^{18}F]AZD4694 SUVR values were estimated to generate a measure of cortical amyloid-β burden based on a composite set of regions including the precuneus, prefrontal, orbitofrontal, parietal, temporal, anterior, and posterior cingulate cortices [66].

Statistical Analysis

Statistical tests relating final imaging measures to clinical measures were performed on Matlab software. LC signal was related to clinical group using ANCOVAs with Tukey's post-hoc tests. LC signal was related to tau burden in the temporal ROI by linear regression with the model:

$$\text{LC signal} = \beta_0 + \beta_1([^{18}\text{F}]\text{MK6240 SUVR in temporal ROI}) + \beta_2(\text{age}) + \beta_3(\text{sex}) + \varepsilon$$

Where LC signal was the average signal in whole LC in some models and the signal for each LC section in others; [^{18}F]MK6240 SUVR was continuous in some models and binary (cutoff =1.24) in others. Partial Spearman correlations were used to relate LC signal to measures of AD severity. Linear regressions and partial Spearman correlations were used to relate NPS severity to LC signal and other neuroimaging measures. The general form for the linear regressions was:

$$\text{NPS severity} = \beta_o + \beta_1(\text{LC signal}) + \beta_{i+1}(\text{neuroimaging measure}_i) \ldots \beta_{n+1}(\text{neuroimaging measure}_n) + \beta_{n+2}(\text{CDR score}) + \beta_{n+3}(\text{age}) + \beta_{n+4}(\text{sex}) + \varepsilon$$

Non-parametric analyses were favored where possible because many measures were ordinal (e.g. CDR score, Braak stage) or not normally distributed according to Lilliefors test (e.g. MMSE score, NPS severity). All analyses controlled for age and sex. See Results for details of the specific models used.

Results

Loss of locus coeruleus signal in AD

First, we confirmed that our novel method of LC signal measurement replicated past reports [7,11-14] of reduced LC signal in clinically-diagnosed AD (clinical-group effect on whole LC signal: $F_{2,185}$ =4.23, p=0.016, 1-way ANCOVA controlling for age and sex). Post-hoc testing found a significant difference between CN and AD (p=0.021) but not between CN and MCI or MCI and AD (p=0.19 and p=0.92 respectively; Tukey's HSD). AD defined biologically by tau positivity ([^{18}F]MK6240 SUVR >1.24 in the temporal ROI [21,66] shown in Figure 2D) was also associated with reduced whole LC signal (t_{186}=-3.26, p=0.0013, Cohen's d=0.48, linear regression controlling for age and sex.

Next, we examined the anatomical topography of tau-associated signal loss within the LC, which we divided into 5 rostrocaudal sections on the left and right side. The middle section and the section below it (encircled sections in Figure 2B-C) showed the greatest signal loss in relation to tau burden in the temporal ROI (linear regression controlling for age and sex; Figure 2B-C). This was true whether tau burden was calculated as a dichotomous or a continuous measure of SUVR in this ROI. LC signal averaged from these sections was markedly reduced in tau positive individuals (t_{186}=-4.00, p=0.0001, Cohen's d=0.59, linear regression controlling for age and sex, Figure 2E). Therefore, we retained this as the LC signal measure to be used for all subsequent analyses, referred to as the 'mid-caudal LC' (Figure 2B-C).

Locus coeruleus signal and AD stage and severity

We found that mid-caudal LC signal loss was significantly correlated to more advanced Braak stage of AD (Spearman ρ=-0.31, p=0.00006, n=160; partial correlations controlling for age and sex; see Figure 2F). Analysis across all stages found that LC signal was lost at the rate of 0.67% CNR per stage, although the rate of loss was higher from stage 3-6, equal to 1.10% CNR/stage (linear regression controlling for age and sex). Consistent with this, general clinical severity, measured as cognitive impairment and dementia severity, was also negatively correlated to LC signal (MMSE errors: ρ=-0.14, p=0.058, n=187; CDR score: ρ=-0.28, p=0.0001, n=188; partial correlations controlling for age and sex; see Figure 2G-H). Taken together, these findings suggest that degeneration of LC may be progressive throughout the early course of AD.

Locus coeruleus signal and symptoms of Alzheimer's disease

We next investigated the clinical correlates of mid-caudal LC signal controlling for key pathophysiological measures to assess the independent contribution of the LC to these measures. First, we tested the relationship of the LC signal to NPS severity (MBI-C total score) in all participants. We found a significant interaction between tau-positivity and LC signal on NPS severity (β_{Int}=0.75, t_{171}=2.76, p=0.006) due to a significant relationship between LC signal and NPS severity in tau positive participants (β_1=0.81, t_{171}=3.36, p=0.0009) but no such relationship in tau negative participants (β_1=0.06, t_{171}=0.42, p=0.67, linear regression controlling for CDR score, age, and sex). We further investigated the LC signal's association with NPS in the tau-positive group (n=51) and found that it was present using parametric or non-parametric statistics and that the association was slightly strengthened when additional pathophysiological measures were included in the model (Table 2; in a full model the correlation of LC signal to MBI total score was ρ=0.35, p=0.019; partial Spearman correlation controlling for tau burden in temporal ROI, cortical amyloid-β burden, cortical gray matter volume, total intracranial volume, CDR score, age, and sex; see Table 2 and Figure 3A-B). This positive correlation is consistent with our hypothesis that preserved and/or elevated LC function is associated with worse NPS. While in most models tau burden in the temporal ROI also significantly predicted higher NPS severity, LC signal was consistently the more influential predictor. Furthermore, the full model including all pathophysiological measures explained a substantial amount of variability in NPS severity (R^2=0.50, adjusted R^2=0.41; Table 2 and Figure 3A). Post-hoc analyses examining MBI-C domains and including the covariates from the full model found the correlation to LC signal was significant only for the impulse dyscontrol domain (ρ=0.44, p=0.0027, Figure 3C). Subsequent examination of all LC sections (Fig 3D) showed the relationship of LC signal to impulse dyscontrol was strongest in the second caudal-most section.

Lastly, we examined the relationship of LC signal to cognitive impairment, measured as errors on the MMSE. Unlike the analysis in the section on AD stage and severity (Figure 2G) we now tested this relationship while controlling for other measures of pathophysiology. We found that this relationship was not significant (ρ=-0.20, p=0.18, n=52, Spearman partial correlation on tau positive participants controlling for covariates as in the full model). This would suggest that LC signal may not have a strong and direct association to general cognitive impairment in AD.

Discussion

Here we report several findings regarding the clinical and pathophysiological correlates of LC signal, a proxy measure of norepinephrine neuron loss, in AD. Loss of LC signal appears to be a progressive process that correlates with AD stage as indexed both by Braak stages of cortical tau proliferation and by severity of clinical symptoms. Despite these detrimental correlates of LC signal loss in AD, *preservation* of LC signal can also be detrimental as it is associated with worse NPS in AD patients. The relationship between LC signal and NPS was not confounded by the presence of cortical pathology; indeed, both LC signal and cortical tau burden independently predicted severity of NPS.

Critically, we found a significant interaction between tau status and LC signal on NPS severity suggesting that tau may dysregulate LC function in a disease-specific way that is distinct from alterations in LC function during normal aging. Specifically, we found no clear relationship between LC signal and NPS severity in healthy individuals. This finding is unsurprising since the level of endorsement of NPS was low in such individuals (Table 1) and furthermore, the

assumption that variability in LC signal can be used as a proxy of the extent of LC degeneration may only apply in the AD/MCI groups, not the healthy group where LC degeneration is minimal and other factors may predominate in determining variability in the LC signal. On the other hand, we found that in tau-positive individuals, a preserved level of LC signal was associated with NPS risk. This is consistent with evidence of a positive relationship between norepinephrine function and NPS in AD [34,36-39,45] (but see [35,71]), suggesting NPS are associated with LC preservation and enhanced norepinephrine function from compensatory changes in norepinephrine production, receptor expression, and number of axon terminals [3,4,42,43]. We propose a model whereby variability in the progression of different disease processes may leave some patients with cortical tau pathology but spared LC integrity, possibly leading to dysregulation in the cortical and subcortical regulation of behavior and the expression of impulse control problems and other NPS. Perhaps the cortical tau insult interferes with top-down regulation of behavioral responses to stressful or arousing situations when the LC-norepinephrine system is intact or hyperactive, leading to agitated or aggressive behavior. Furthermore, NPS may be promoted not only by interaction of LC signal with cortical tau, but also with tau in the LC itself, which cannot be measured with PET imaging due the size of the LC but would be expected to be present in those with cortical tau [2-4] and could dysregulate LC function.

These findings are consistent with prior reports showing efficacy of norepinephrine blocking agents against aggressive and agitated behaviors in AD [38-40]. NM-MRI could have promise in this regard as a biomarker to indicate patients with high LC signal whose NPS may respond to such treatment, as opposed to patients with low LC signal whose NPS may have an origin unrelated to the norepinephrine system and who could be harmed by treatments exacerbating their already low norepinephrine system function. Furthermore, while NPS are often recognizable by clinical observation alone, a biological measure such as LC signal could show promise as a biomarker of NPS risk prior to their overt manifestation. Such a risk marker would be important for clinical decision-making, supporting vigilance of emergent NPS, and allowing administration of NPS treatments at the earliest stages, even during the prodrome.

Our findings provide insight regarding the anatomical topography and timing of LC signal loss in AD. Consistent with reports of a highly variable extent of LC cell loss in AD [61], we observed a large variability in LC signal loss (Figure 2E). LC signal loss was most pronounced in central LC, consistent with this region having the greatest density of norepinephrine cells and the greatest number of cells lost in AD [61]. This anatomical variability underscores the strengths of our ‘funnel tip’ LC signal measurement approach, allowing automated determination of approximate rostrocaudal position within the LC, while still extracting the signal from unprocessed images to avoid distortion of this small structure. This approach has the promise to target specific effects that may be anatomically segregated from other, potentially confounding, effects. For instance, we saw the tau effect was strongest in the middle LC section, whereas the NPS effect was strongest in the section below the middle (Figures 2B, 2C and 3D). Such a subdivision of the LC could help probe specific circuits that may be subserved by distinct LC regions, consistent with recent work demonstrating a modular organization of LC circuitry [72]. Yet, despite this organization, distinct modules tend to be intermingled and more research is needed to determine the extent of any topographical pattern to LC projections in primates [72-75]. Thus, it may be premature to provide an explanation for why caudal LC would be

specifically linked to impulse control symptoms and whether this is due to the connectivity of this subregion [73] or perhaps the degree to which it is vulnerable to degeneration [61].

Regarding the timing of LC signal loss in AD, mirroring post-mortem evidence [1], we found LC signal loss to be a gradual process across Braak stages. This suggests that there is substantial delay between the accumulation of tau in the LC at the earliest stage of AD [3,4] and the degeneration of LC neurons. Nevertheless, close examination of the relationship between LC signal and Braak stage (Figure 2F) shows a curious phenomenon where LC signal is low at Braak stage 1 and appears to increase from Braak stage 1-3. Although this may be simply due to a low number of observations (e.g. at Braak stage 3), such a rebound in LC signal could reflect a biological process linked to a hyperactive LC-norepinephrine system post-degeneration [2,3,36]. For instance this could lead to increased cell size, or accelerated neuromelanin accumulation, changes that could increase the LC signal [5,76]. Indeed, a correlation of NM signal to catecholamine function has been observed in the dopamine system [58]. In this speculative scenario, it could be that loss of NM-MRI signal is apparent even at Braak stage 1 (when LC signal was significantly reduced relative to Braak stage 0, $t_{88}=2.36$, $p=0.020$) but that reductions in LC NM-MRI signal due to degeneration become somewhat confounded by increases in NM-MRI signal due to hyperactivity during intermediate Braak stages. While this would add noise when NM-MRI is used as a marker of early LC degeneration, it may enhance its sensitivity as a marker of NPS, which may be exacerbated not only by preservation but also hyperactivity of the LC [34,36-40,45].

Our study had many strengths including a relatively large sample and inclusion of multimodal neuroimaging measures of pathophysiology. However, certain methodological aspects may limit interpretation of the data. Our study supported a role for the norepinephrine system in NPS but function of other neurotransmitter systems (e.g. acetylcholine, serotonin) may also play an important role in NPS [36,77] but was not measured. We found that combining measures of cortical and LC pathology explained a substantial amount of variance in NPS severity; however, a detailed examination of the role of the cortical measures in promoting NPS was beyond the scope of this work. We do not interpret, for instance, the absence of a relationship between our measure of cortical amyloid-β burden and NPS as being in conflict with prior studies targeted to specific brain regions and types of NPS [78]. Indeed, NPS are a heterogeneous combination of symptoms and it may be overly simplistic to expect LC signal or any measure to predict all NPS domains, some of which could even be associated with *low* LC signal [46]. One domain, psychotic symptoms, are of interest but could not be investigated in our sample due to very low level of endorsement. We focused on early stages of AD (CDR <3, with CDR for most AD cases <2) and cannot draw conclusions regarding the role of the LC in moderate to severe dementia. At these later stages, perhaps the influence of compensatory increases in norepinephrine function on NPS could be overwhelmed by a more advanced degeneration of the system. Indeed, some preclinical work suggests that with more advanced LC damage, NPS-like behavior begins to diminish [79]. Arguing against this, some post-mortem studies (where cases are highly advanced) have found a positive relationship between antemortem NPS and norepinephrine function [24,35-37]. A detailed assessment of cognition in AD was beyond the scope of this paper but future work could test whether the association seen between LC signal and specific cognitive domains in healthy aging [80] also applies in AD. Finally, our MRI data, like most published LC NM-MRI studies [7,11-14,47] was collected on a 3 Tesla scanner. Ideally, a 7 Tesla scanner [81] would be used due the increased spatial resolution afforded at ultra-high field

strength. At the resolution employed here, measurement of LC signal may have been subject to partial volume effects in which LC voxels contain non-LC tissue. Nonetheless, the in-plane resolution was much smaller than the area of the LC (in-plane area of one voxel=0.47 mm^2, cross-sectional area of the LC ~1.8 mm^2 [61]), the LC could be clearly identified on visual inspection, was segmented with 98% accuracy by our algorithm, and our LC signal measure revealed highly significant effects, in line with *a priori* hypotheses.

In summary, the LC signal tracks Braak stage of AD and is positively correlated to the severity of NPS, independently of other aspects of pathophysiology. These results demonstrate the utility of NM-MRI to interrogate the role of the norepinephrine system in human studies of AD pathophysiology. They also provide early evidence in favor of NM-MRI as a practical and non-invasive biomarker that could have potential to indicate NPS risk or likelihood of response to specific treatments.

Acknowledgments

The authors thank all participants of the study and staff of the McGill Center for studies in Aging. We thank Dean Jolly, Alexey Kostikov, Robert Hopewell, Monica Samoila-Lactatus, Karen Ross, Marina Kostikova, Mehdi Boudjemeline, and Sandy Li for assist in the radiochemistry production. We also thank Richard Strauss, Edith Strauss, Jenna Stevenson, Nesrine Rahmouni, Guylaine Gagne, Carley Mayhew, Alyssa Stevenson, Tasha Vinet-Celluci, Meong Jin Joung, Hung-Hsin Hsiao, Reda Bouhachi, and Arturo Aliaga for consenting subjects and/or for their role in data acquisition. We thank the Cerveau Technologies for the use of MK6240.

Funding

This research is supported by the Weston Brain Institute, Canadian Institutes of Health Research (CIHR) (MOP-11-51-31, FRN, 152985, PI: P.R-N.), the Alzheimer's Association (NIRG-12-92090, NIRP-12-259245, P.R-N.), Fonds de Recherche du Quebec – Santé (FRQS; Chercheur Boursier, P.R-N. and 2020-VICO-279314). P.R-N., S.G., and T.P. are members of the CIHR-CCNA Canadian Consortium of Neurodegeneration in Aging. Canada Foundation for innovation. Project 34874. CFI Project 34874.

Author contributions

CMC, PR-N, JT TAP, ZI made substantial contributions to the conception and design of the work, to the acquisition, analysis, or interpretation of data for the work; and to drafting of the work and revising it critically for important intellectual content. MS, MC, FL SG contributed to collection of neuroimaging and/or clinical data. GM, J-PS, CT contributed to implementation and analysis of neuroimaging measures. VC, LT, AM, SC contributed to data processing and analysis. DW contributed to interpretation of results. All authors contributed to writing and editing the manuscript.

Competing interests

The authors report no competing financial interest in relation to the study design, results, or discussion. C.M.C. and P.R-N are inventors on a pending patent using the analysis method described here, licensed to Terran Biosciences, but have received no royalties.

References

1 Theofilas P, Ehrenberg AJ, Dunlop S, Di Lorenzo Alho AT, Nguy A, Leite REP, et al. Locus coeruleus volume and cell population changes during Alzheimer's disease progression: A stereological study in human postmortem brains with potential implication for early-stage biomarker discovery. Alzheimers Dement. 2017;13(3):236-46.

2 Weinshenker D. Long Road to Ruin: Noradrenergic Dysfunction in Neurodegenerative Disease. Trends Neurosci. 2018;41(4):211-23.

3 Gannon M, Che P, Chen Y, Jiao K, Roberson ED, Wang Q. Noradrenergic dysfunction in Alzheimer's disease. Front Neurosci. 2015;9:220.

4 Satoh A, Iijima KM. Roles of tau pathology in the locus coeruleus (LC) in age-associated pathophysiology and Alzheimer's disease pathogenesis: Potential strategies to protect the LC against aging. Brain Res. 2019;1702:17-28.

5 Sulzer D, Cassidy C, Horga G, Kang UJ, Fahn S, Casella L, et al. Neuromelanin detection by magnetic resonance imaging (MRI) and its promise as a biomarker for Parkinson's disease. NPJ Parkinsons Dis. 2018;4:11.

6 Keren NI, Taheri S, Vazey EM, Morgan PS, Granholm AC, Aston-Jones GS, et al. Histologic validation of locus coeruleus MRI contrast in post-mortem tissue. Neuroimage. 2015;113:235-45.

7 Kelberman M, Keilholz S, Weinshenker D. What's That (Blue) Spot on my MRI? Multimodal Neuroimaging of the Locus Coeruleus in Neurodegenerative Disease. Front Neurosci. 2020;14:583421.

8 Jacobs HIL, Becker JA, Kwong K, Engels-Dominguez N, Prokopiou PC, Papp KV, et al. In vivo and neuropathology data support locus coeruleus integrity as indicator of Alzheimer's disease pathology and cognitive decline. Sci Transl Med. 2021;13(612):eabj2511.

9 Watanabe T, Tan Z, Wang X, Martinez-Hernandez A, Frahm J. Magnetic resonance imaging of noradrenergic neurons. Brain Struct Funct. 2019;224(4):1609-25.

10 Sommerauer M, Fedorova TD, Hansen AK, Knudsen K, Otto M, Jeppesen J, et al. Evaluation of the noradrenergic system in Parkinson's disease: an 11C-MeNER PET and neuromelanin MRI study. Brain. 2018;141(2):496-504.

11 Olivieri P, Lagarde J, Lehericy S, Valabregue R, Michel A, Mace P, et al. Early alteration of the locus coeruleus in phenotypic variants of Alzheimer's disease. Ann Clin Transl Neurol. 2019;6(7):1345-51.

12 Dordevic M, Muller-Fotti A, Muller P, Schmicker M, Kaufmann J, Muller NG. Optimal Cut-Off Value for Locus Coeruleus-to-Pons Intensity Ratio as Clinical Biomarker for Alzheimer's Disease: A Pilot Study. J Alzheimers Dis Rep. 2017;1(1):159-67.

13 Takahashi J, Shibata T, Sasaki M, Kudo M, Yanezawa H, Obara S, et al. Detection of changes in the locus coeruleus in patients with mild cognitive impairment and Alzheimer's disease: high-resolution fast spin-echo T1-weighted imaging. Geriatr Gerontol Int. 2015;15(3):334-40.

14 Hou R, Beardmore R, Holmes C, Osmond C, Darekar A. A case-control study of the locus coeruleus degeneration in Alzheimer's disease. Eur Neuropsychopharmacol. 2021;43:153-59.

15 Betts MJ, Cardenas-Blanco A, Kanowski M, Spottke A, Teipel SJ, Kilimann I, et al. Locus coeruleus MRI contrast is reduced in Alzheimer's disease dementia and correlates with CSF Abeta levels. Alzheimers Dement (Amst). 2019;11:281-85.

16 Aguero C, Dhaynaut M, Normandin MD, Amaral AC, Guehl NJ, Neelamegam R, et al. Autoradiography validation of novel tau PET tracer [F-18]-MK-6240 on human postmortem brain tissue. Acta Neuropathol Commun. 2019;7(1):37.

17 Rowe CC, Pejoska S, Mulligan RS, Jones G, Chan JG, Svensson S, et al. Head-to-head comparison of 11C-PiB and 18F-AZD4694 (NAV4694) for β-amyloid imaging in aging and dementia. J Nucl Med. 2013;54(6):880-6.
18 Therriault J, Benedet A, Pascoal TA, Savard M, Ashton N, Chamoun M, et al. Determining Amyloid-beta positivity using [(18)F]AZD4694 PET imaging. J Nucl Med. 2020.
19 Lussier FZ, Pascoal TA, Chamoun M, Therriault J, Tissot C, Savard M, et al. Mild behavioral impairment is associated with β-amyloid but not tau or neurodegeneration in cognitively intact elderly individuals. Alzheimers Dement. 2020;16(1):192-99.
20 Jellinger KA, Bancher C. Neuropathology of Alzheimer's disease: a critical update. J Neural Transm Suppl. 1998;54:77-95.
21 Therriault J, Pascoal TA, Benedet AL, Tissot C, Savard M, Chamoun M, et al. Frequency of Biologically Defined Alzheimer Disease in Relation to Age, Sex, APOE epsilon4, and Cognitive Impairment. Neurology. 2021;96(7):e975-e85.
22 Pascoal TA, Therriault J, Benedet AL, Savard M, Lussier FZ, Chamoun M, et al. 18F-MK-6240 PET for early and late detection of neurofibrillary tangles. Brain. 2020;143(9):2818-30.
23 Braun D, Feinstein DL. The locus coeruleus neuroprotective drug vindeburnol normalizes behavior in the 5xFAD transgenic mouse model of Alzheimer's disease. Brain Res. 2019;1702:29-37.
24 Herrmann N, Lanctot KL, Khan LR. The role of norepinephrine in the behavioral and psychological symptoms of dementia. J Neuropsychiatry Clin Neurosci. 2004;16(3):261-76.
25 Lanctot KL, Amatniek J, Ancoli-Israel S, Arnold SE, Ballard C, Cohen-Mansfield J, et al. Neuropsychiatric signs and symptoms of Alzheimer's disease: New treatment paradigms. Alzheimers Dement (N Y). 2017;3(3):440-49.
26 Hwang TJ, Masterman DL, Ortiz F, Fairbanks LA, Cummings JL. Mild cognitive impairment is associated with characteristic neuropsychiatric symptoms. Alzheimer Dis Assoc Disord. 2004;18(1):17-21.
27 Gatchel JR, Donovan NJ, Locascio JJ, Schultz AP, Becker JA, Chhatwal J, et al. Depressive Symptoms and Tau Accumulation in the Inferior Temporal Lobe and Entorhinal Cortex in Cognitively Normal Older Adults: A Pilot Study. J Alzheimers Dis. 2017;59(3):975-85.
28 Wise EA, Rosenberg PB, Lyketsos CG, Leoutsakos JM. Time course of neuropsychiatric symptoms and cognitive diagnosis in National Alzheimer's Coordinating Centers volunteers. Alzheimers Dement (Amst). 2019;11:333-39.
29 Lyketsos CG, Carrillo MC, Ryan JM, Khachaturian AS, Trzepacz P, Amatniek J, et al. Neuropsychiatric symptoms in Alzheimer's disease. Alzheimers Dement. 2011;7(5):532-9.
30 Allegri RF, Sarasola D, Serrano CM, Taragano FE, Arizaga RL, Butman J, et al. Neuropsychiatric symptoms as a predictor of caregiver burden in Alzheimer's disease. Neuropsychiatr Dis Treat. 2006;2(1):105-10.
31 Nelson JC, Delucchi K, Schneider LS. Efficacy of second generation antidepressants in late-life depression: a meta-analysis of the evidence. Am J Geriatr Psychiatry. 2008;16(7):558-67.
32 Schneider LS, Dagerman K, Insel PS. Efficacy and adverse effects of atypical antipsychotics for dementia: meta-analysis of randomized, placebo-controlled trials. Am J Geriatr Psychiatry. 2006;14(3):191-210.
33 Weintraub D, Rosenberg PB, Drye LT, Martin BK, Frangakis C, Mintzer JE, et al. Sertraline for the treatment of depression in Alzheimer disease: week-24 outcomes. Am J Geriatr Psychiatry. 2010;18(4):332-40.
34 Jacobs HIL, Riphagen JM, Ramakers IHGB, Verhey FRJ. Alzheimer's disease pathology: pathways between central norepinephrine activity, memory, and neuropsychiatric symptoms. Mol Psychiatry. 2019.

35 Vermeiren Y, Van Dam D, Aerts T, Engelborghs S, De Deyn PP. Brain region-specific monoaminergic correlates of neuropsychiatric symptoms in Alzheimer's disease. J Alzheimers Dis. 2014;41(3):819-33.
36 Liu KY, Stringer AE, Reeves SJ, Howard RJ. The neurochemistry of agitation in Alzheimer's disease: a systematic review. Ageing Res Rev. 2018;43:99-107.
37 Sharp SI, Ballard CG, Chen CP, Francis PT. Aggressive behavior and neuroleptic medication are associated with increased number of alpha1-adrenoceptors in patients with Alzheimer disease. Am J Geriatr Psychiatry. 2007;15(5):435-7.
38 Herrmann N, Lanctot KL, Eryavec G, Khan LR. Noradrenergic activity is associated with response to pindolol in aggressive Alzheimer's disease patients. J Psychopharmacol. 2004;18(2):215-20.
39 Peskind ER, Tsuang DW, Bonner LT, Pascualy M, Riekse RG, Snowden MB, et al. Propranolol for disruptive behaviors in nursing home residents with probable or possible Alzheimer disease: a placebo-controlled study. Alzheimer Dis Assoc Disord. 2005;19(1):23-8.
40 Wang LY, Shofer JB, Rohde K, Hart KL, Hoff DJ, McFall YH, et al. Prazosin for the treatment of behavioral symptoms in patients with Alzheimer disease with agitation and aggression. Am J Geriatr Psychiatry. 2009;17(9):744-51.
41 Teri L, Reifler BV, Veith RC, Barnes R, White E, McLean P, et al. Imipramine in the treatment of depressed Alzheimer's patients: impact on cognition. J Gerontol. 1991;46(6):P372-7.
42 Szot P, Leverenz JB, Peskind ER, Kiyasu E, Rohde K, Miller MA, et al. Tyrosine hydroxylase and norepinephrine transporter mRNA expression in the locus coeruleus in Alzheimer's disease. Brain Res Mol Brain Res. 2000;84(1-2):135-40.
43 Szot P, White SS, Greenup JL, Leverenz JB, Peskind ER, Raskind MA. Compensatory changes in the noradrenergic nervous system in the locus ceruleus and hippocampus of postmortem subjects with Alzheimer's disease and dementia with Lewy bodies. J Neurosci. 2006;26(2):467-78.
44 Elrod R, Peskind ER, DiGiacomo L, Brodkin KI, Veith RC, Raskind MA. Effects of Alzheimer's disease severity on cerebrospinal fluid norepinephrine concentration. Am J Psychiatry. 1997;154(1):25-30.
45 Zubenko GS, Moossy J, Martinez AJ, Rao G, Claassen D, Rosen J, et al. Neuropathologic and neurochemical correlates of psychosis in primary dementia. Arch Neurol. 1991;48(6):619-24.
46 Sasaki M, Shibata E, Ohtsuka K, Endoh J, Kudo K, Narumi S, et al. Visual discrimination among patients with depression and schizophrenia and healthy individuals using semiquantitative color-coded fast spin-echo T1-weighted magnetic resonance imaging. Neuroradiology. 2010;52(2):83-9.
47 Garcia-Lorenzo D, Longo-Dos Santos C, Ewenczyk C, Leu-Semenescu S, Gallea C, Quattrocchi G, et al. The coeruleus/subcoeruleus complex in rapid eye movement sleep behaviour disorders in Parkinson's disease. Brain. 2013;136(Pt 7):2120-9.
48 Mather M, Joo Yoo H, Clewett DV, Lee TH, Greening SG, Ponzio A, et al. Higher locus coeruleus MRI contrast is associated with lower parasympathetic influence over heart rate variability. Neuroimage. 2017;150:329-35.
49 Krell-Roesch J, Vassilaki M, Mielke MM, Kremers WK, Lowe VJ, Vemuri P, et al. Cortical β-amyloid burden, neuropsychiatric symptoms, and cognitive status: the Mayo Clinic Study of Aging. Transl Psychiatry. 2019;9(1):123.
50 Van Dam D, Vermeiren Y, Dekker AD, Naude PJ, Deyn PP. Neuropsychiatric Disturbances in Alzheimer's Disease: What Have We Learned from Neuropathological Studies? Curr Alzheimer Res. 2016;13(10):1145-64.

51 Showraki A, Murari G, Ismail Z, Barfett JJ, Fornazzari L, Munoz DG, et al. Cerebrospinal Fluid Correlates of Neuropsychiatric Symptoms in Patients with Alzheimer's Disease/Mild Cognitive Impairment: A Systematic Review. J Alzheimers Dis. 2019;71(2):477-501.
52 Ismail Z, Aguera-Ortiz L, Brodaty H, Cieslak A, Cummings J, Fischer CE, et al. The Mild Behavioral Impairment Checklist (MBI-C): A Rating Scale for Neuropsychiatric Symptoms in Pre-Dementia Populations. J Alzheimers Dis. 2017;56(3):929-38.
53 Cui Y, Dai S, Miao Z, Zhong Y, Liu Y, Liu L, et al. Reliability and Validity of the Chinese Version of the Mild Behavioral Impairment Checklist for Screening for Alzheimer's Disease. J Alzheimers Dis. 2019;70(3):747-56.
54 Mallo SC, Ismail Z, Pereiro AX, Facal D, Lojo-Seoane C, Campos-Magdaleno M, et al. Assessing Mild Behavioral Impairment with the Mild Behavioral Impairment-Checklist in People with Mild Cognitive Impairment. J Alzheimers Dis. 2018;66(1):83-95.
55 Therriault J, Benedet AL, Pascoal TA, Mathotaarachchi S, Chamoun M, Savard M, et al. Association of Apolipoprotein E epsilon4 With Medial Temporal Tau Independent of Amyloid-beta. JAMA Neurol. 2020;77(4):470-79.
56 McKhann GM, Knopman DS, Chertkow H, Hyman BT, Jack CR, Kawas CH, et al. The diagnosis of dementia due to Alzheimer's disease: recommendations from the National Institute on Aging-Alzheimer's Association workgroups on diagnostic guidelines for Alzheimer's disease. Alzheimers Dement. 2011;7(3):263-9.
57 Jacobs HI, Priovoulos N, Poser BA, Pagen LH, Ivanov D, Verhey FR, et al. Dynamic behavior of the locus coeruleus during arousal-related memory processing in a multi-modal 7T fMRI paradigm. Elife. 2020;9.
58 Cassidy CM, Zucca FA, Girgis RR, Baker SC, Weinstein JJ, Sharp ME, et al. Neuromelanin-sensitive MRI as a noninvasive proxy measure of dopamine function in the human brain. Proc Natl Acad Sci U S A. 2019;116(11):5108-17.
59 Wengler K, Ashinoff BK, Pueraro E, Cassidy CM, Horga G, Rutherford BR. Association between neuromelanin-sensitive MRI signal and psychomotor slowing in late-life depression. Neuropsychopharmacology. 2020.
60 Naidich TP, Duvernoy HM, Delman BN, Sorensen AG, Kollias SS, Haacke ME. Duvernoy's atlas of the human brain stem and cerebellum : high-field MRI : surface anatomy, internal structure, vascularization and 3D sectional anatomy. Springer: Wien ; New York; 2009.
61 German DC, Manaye KF, White CL, 3rd, Woodward DJ, McIntire DD, Smith WK, et al. Disease-specific patterns of locus coeruleus cell loss. Ann Neurol. 1992;32(5):667-76.
62 Chen X, Huddleston DE, Langley J, Ahn S, Barnum CJ, Factor SA, et al. Simultaneous imaging of locus coeruleus and substantia nigra with a quantitative neuromelanin MRI approach. Magn Reson Imaging. 2014;32(10):1301-6.
63 Pascoal TA, Shin M, Kang MS, Chamoun M, Chartrand D, Mathotaarachchi S, et al. In vivo quantification of neurofibrillary tangles with [(18)F]MK-6240. Alzheimers Res Ther. 2018;10(1):74.
64 Cselényi Z, Jönhagen ME, Forsberg A, Halldin C, Julin P, Schou M, et al. Clinical validation of 18F-AZD4694, an amyloid-β-specific PET radioligand. J Nucl Med. 2012;53(3):415-24.
65 Mazziotta JC, Toga AW, Evans A, Fox P, Lancaster J. A probabilistic atlas of the human brain: theory and rationale for its development. The International Consortium for Brain Mapping (ICBM). Neuroimage. 1995;2(2):89-101.
66 Jack CR, Jr., Wiste HJ, Weigand SD, Therneau TM, Lowe VJ, Knopman DS, et al. Defining imaging biomarker cut points for brain aging and Alzheimer's disease. Alzheimers Dement. 2017;13(3):205-16.

67 Braak H, Braak E. Neuropathological stageing of Alzheimer-related changes. Acta Neuropathol. 1991;82(4):239-59.
68 Braak H, Braak E. Frequency of stages of Alzheimer-related lesions in different age categories. Neurobiol Aging. 1997;18(4):351-7.
69 Braak H, Alafuzoff I, Arzberger T, Kretzschmar H, Del Tredici K. Staging of Alzheimer disease-associated neurofibrillary pathology using paraffin sections and immunocytochemistry. Acta Neuropathol. 2006;112(4):389-404.
70 Braak H, Thal DR, Ghebremedhin E, Del Tredici K. Stages of the pathologic process in Alzheimer disease: age categories from 1 to 100 years. J Neuropathol Exp Neurol. 2011;70(11):960-9.
71 Matthews KL, Chen CP, Esiri MM, Keene J, Minger SL, Francis PT. Noradrenergic changes, aggressive behavior, and cognition in patients with dementia. Biol Psychiatry. 2002;51(5):407-16.
72 Poe GR, Foote S, Eschenko O, Johansen JP, Bouret S, Aston-Jones G, et al. Locus coeruleus: a new look at the blue spot. Nat Rev Neurosci. 2020;21(11):644-59.
73 Hirschberg S, Li Y, Randall A, Kremer EJ, Pickering AE. Functional dichotomy in spinal- vs prefrontal-projecting locus coeruleus modules splits descending noradrenergic analgesia from ascending aversion and anxiety in rats. Elife. 2017;6.
74 Samuels ER, Szabadi E. Functional neuroanatomy of the noradrenergic locus coeruleus: its roles in the regulation of arousal and autonomic function part II: physiological and pharmacological manipulations and pathological alterations of locus coeruleus activity in humans. Curr Neuropharmacol. 2008;6(3):254-85.
75 Gatter KC, Powell TP. The projection of the locus coeruleus upon the neocortex in the macaque monkey. Neuroscience. 1977;2(3):441-5.
76 Priovoulos N, van Boxel SCJ, Jacobs HIL, Poser BA, Uludag K, Verhey FRJ, et al. Unraveling the contributions to the neuromelanin-MRI contrast. Brain Struct Funct. 2020;225(9):2757-74.
77 Grossberg GT. Effect of rivastigmine in the treatment of behavioral disturbances associated with dementia: review of neuropsychiatric impairment in Alzheimer's disease. Curr Med Res Opin. 2005;21(10):1631-9.
78 Lussier FZ, Pascoal TA, Chamoun M, Therriault J, Tissot C, Savard M, et al. Mild behavioral impairment is associated with beta-amyloid but not tau or neurodegeneration in cognitively intact elderly individuals. Alzheimers Dement. 2020;16(1):192-99.
79 Szot P, Franklin A, Miguelez C, Wang Y, Vidaurrazaga I, Ugedo L, et al. Depressive-like behavior observed with a minimal loss of locus coeruleus (LC) neurons following administration of 6-hydroxydopamine is associated with electrophysiological changes and reversed with precursors of norepinephrine. Neuropharmacology. 2016;101:76-86.
80 Elman JA, Puckett OK, Beck A, Fennema-Notestine C, Cross LK, Dale AM, et al. MRI-assessed locus coeruleus integrity is heritable and associated with multiple cognitive domains, mild cognitive impairment, and daytime dysfunction. Alzheimers Dement. 2021.
81 Priovoulos N, Jacobs HIL, Ivanov D, Uludag K, Verhey FRJ, Poser BA. High-resolution in vivo imaging of human locus coeruleus by magnetization transfer MRI at 3T and 7T. Neuroimage. 2018;168:427-36.

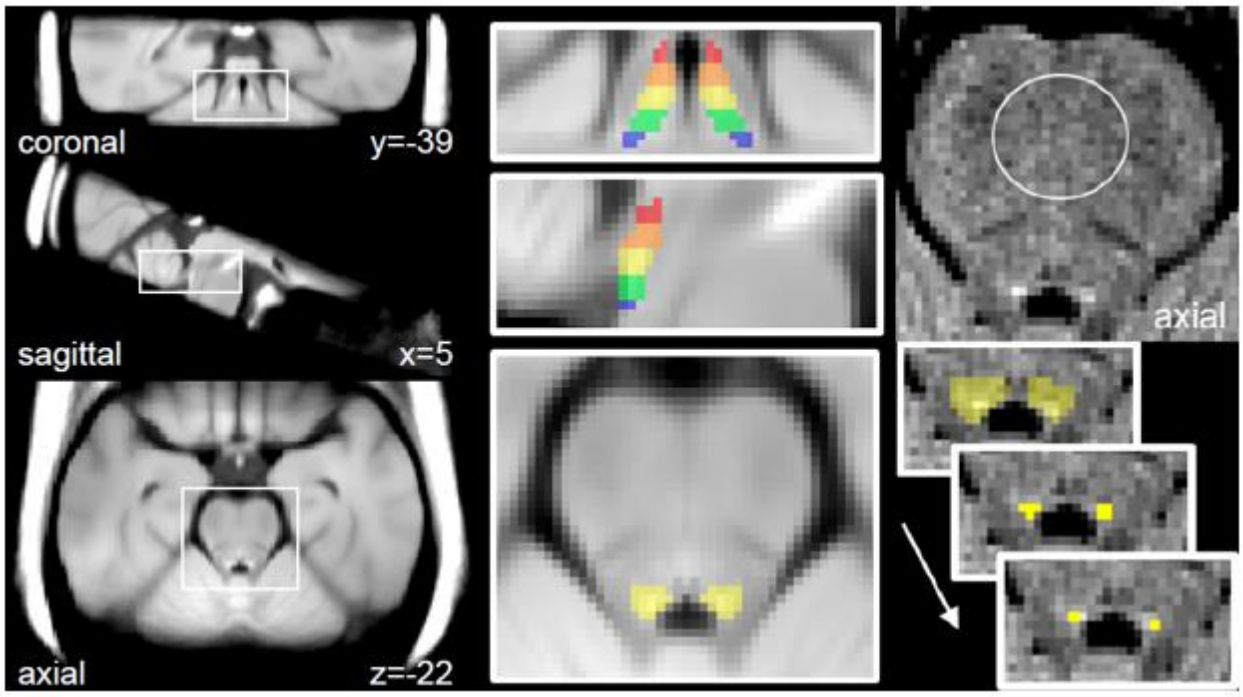

Figure. 1. Measurement of LC signal. Left: visualization template in MNI space created by averaging the spatially normalized NM-MRI images from all participants. Middle: magnified views of the visualization template with the LC search mask overlaid. This mask was manually traced on the visualization template over the hyperintense region surrounding the LC and divided into 5 sections (displayed in different colors), each spanning 3 mm in the z-axis. Top-right: unprocessed NM-MRI image showing the pons of a representative individual; the central pons reference region is encircled in white. Contrast-to-noise ratio for all voxels was calculated relative to signal extracted from this region. Bottom-right: segmentation of the LC in native space. The LC search mask (yellow, signifying the middle section) was deformed from MNI space to native space to provide a search space wherein the LC was identified on left and right sides as the 4 adjacent voxels with highest signal contrast. To minimize partial volume effects, of these 4, only the peak-contrast voxel was retained for each side and slice. LC signal was calculated per section by averaging CNR values from all such voxels within the section.

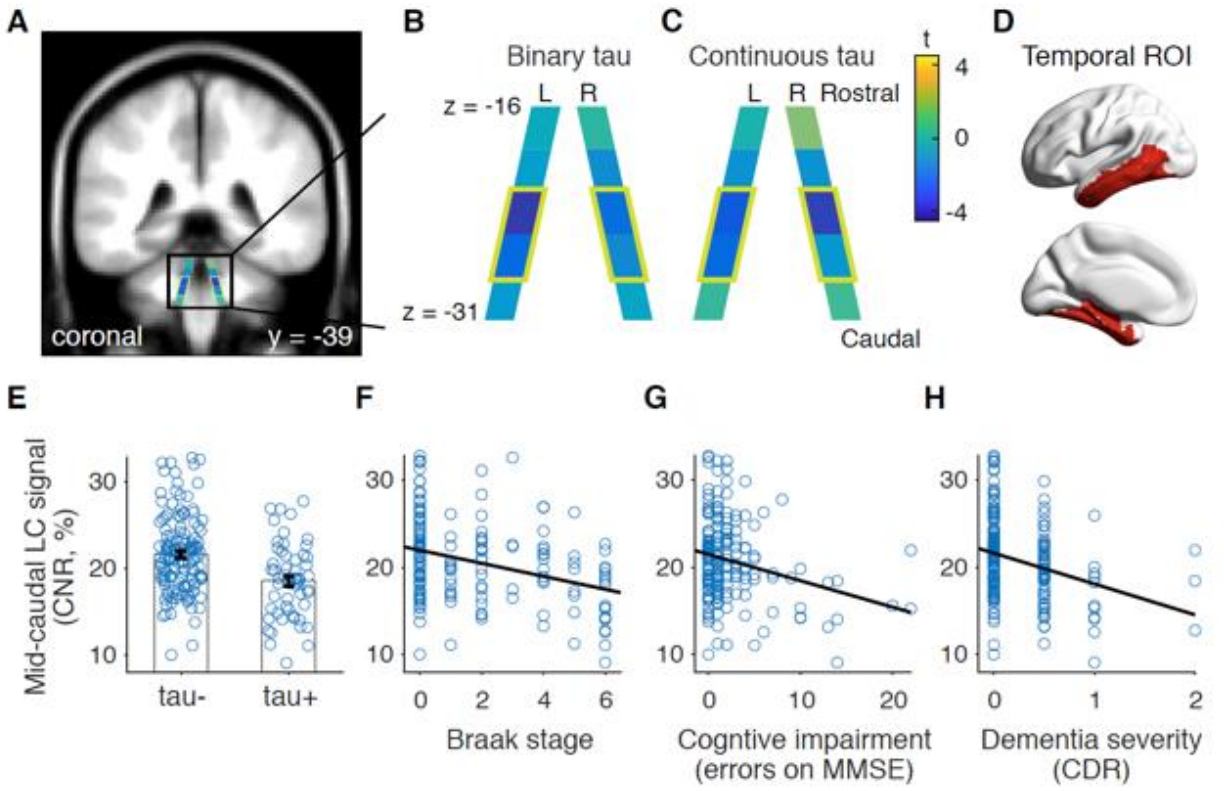

Figure. 2. LC signal and AD severity. (**A-C**): schematic representations of the LC. (**A**) LC schematic overlaid on anatomical template in coronal view to illustrate position in the brain. (**B-C**) LC schematic showing signal loss in each of the rostro-caudal sections based on tau burden in the temporal ROI (left hemisphere shown in **D,** right hemisphere is similar). In (**B)** tau burden was dichotomized ([^{18}F]MK6240 SUVR>1.24 to define tau positive cases) and in (**C**) it was left as a continuous measure. The strongest relationship was seen in the mid-caudal LC sections (MNI space z coordinate = -28 to -22; encircled in chartreuse green and matching the yellow and green LC sections shown in Figure 1). Bilateral LC signal from these sections was retained as the metric used for subsequent analyses of LC signal. (**E-H**): Scatterplots showing relationship of mid-caudal LC signal to tau status (E) and measures of AD severity including Braak stage as determined with [^{18}F]MK6240 PET imaging (**F**), cognitive impairment (**G**), and dementia severity (**H**). L: left, R: right, MMSE: Mini Mental State Exam, CDR: Clinical Dementia Rating Scale.

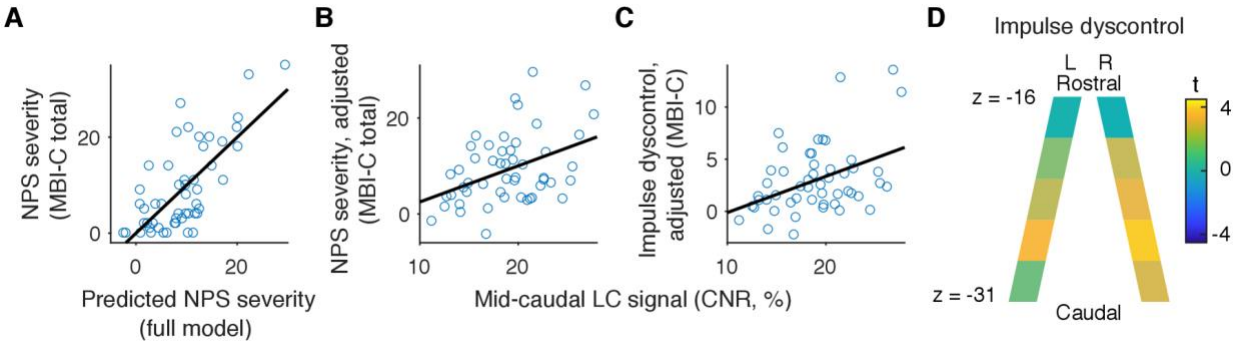

Figure 3. Relationship between mid-caudal LC signal and neuropsychiatric symptom severity in n=51 tau-positive older adults. (**A**) Neuropsychiatric symptom severity was strongly predicted in a linear regression model combining several multimodal neuroimaging measures of pathophysiology ('full model' in Table 2), including LC signal, tau burden in the temporal ROI, cortical amyloid-β burden, and cortical gray matter volume (adj. R^2=0.41). The most influential predictor in this model was LC signal, which was positively correlated to NPS severity (**B**). Of the 5 domains of NPS, LC signal was most strongly correlated to the Impulse Dyscontrol domain (**C**). NPS severity score was adjusted in **B** and **C** based on other covariates in the model. (**D**) LC schematic showing correlation of LC signal to impulse control deficits for all rostro-caudal LC sections (controlling for covariates as in 'full model').

Table 1: Clinical and demographic measures

Characteristic	CN (n = 118)	MCI (n = 44)	AD (n = 28)	*P* Value		
				CN vs. AD	CN vs. MCI	MCI vs. AD
Age, mean (SD), y	72.3 (5.7)	73.2 (5.4)	67.4 (8.9)	<0.001	0.70	0.03
Male, No. (%)	36 (30.5)	21 (47.7)	12 (42.9)	0.21	0.03	0.62
Education, mean (SD), y	15.5 (3.6)	14.1 (3.4)	15.0 (3.7)	0.54	0.07	0.46
CDR score, mean (SD)	0.0 (0)	0.5 (0)	0.9 (0.5)	<0.001	n/a	<0.001
MMSE score, mean (SD)	29.2 (0.9)	28.0 (1.8)	20.9 (5.9)	<0.001	<0.001	<0.001
MBI score, mean (SD)	2.3 (5.5)	7.6(8.5)	13.0 (9.8)	<0.001	<0.001	0.04
Tau-positive, No. (%)	10 (8.5)	22 (48.9)	25 (89.3)	<0.001	<0.001	<0.001

p-values are from t-tests for continuous measures and chi-square tests for categorical measures

Table 2: Prediction of neuropsychiatric symptom severity (MBI-C total score) in tau-positive individuals

Dependent variable	Predictors in model, n	R^2	Adj R^2	t-statistic for regression coefficient					Spearman partial correlation, ρ
				Mid-caudal LC signal	Tau-PET, temporal ROI	Cortical amyloid-PET	Cortical gray matter volume	CDR	Mid-caudal LC signal
MBI, total score	4,51	0.44	0.39	2.85**	excluded	excluded	excluded	4.99***	0.32*
	5; 51	0.49	0.44	3.30**	2.25*	excluded	excluded	2.99**	0.35*
	6; 51	0.50	0.43	3.23**	2.08*	0.52	excluded	2.97**	0.35*
	8; 51 (full model)	0.51	0.41	3.31**	1.70	0.63	-0.42	2.70*	0.35*
MBI, impulse dyscontrol	8; 51	0.36	0.24	3.32**	1.70	1.07	-1.10	0.24	0.44**

All analyses included age and sex as covariates. Analysis including cortical gray matter volume also included estimated total intracranial volume as a covariate. *p<0.05, **p<0.01, ***p<0.001